62-1-6

XEROX

THERM ADVANCED RESEARCH

DIVISION OF

THERM

ITHACA, NEW YORK

GENERAL HARMONIC SOLUTIONS FOR THE DUCTED PROPELLER

by

D. E. Ordway and M. D. Greenberg

TAR-TR 613 August 1961

Submitted to Air Programs, Office of Naval Research in partial fulfillment of Contract Nonr-2859(00)

Donald Earl Ordway

Donald Earl Ordway
Head, Aerophysics Section

Approved:

H. S. Tan

H. S. Tan
Scientific Advisor

A. Ritter

A. Ritter
Director, Therm Advanced Research

ACKNOWLEDGMENT

The authors wish to extend their appreciation to Mr. T. Wilson, LCDR A. Van Tuyl and Lt. Col. J. Wosser, Office of Naval Research, for contract administration; to Trinna Iacovelli for report preparation; to G. R. Hough, A. Kaskel and M. M. Sluyter for numerical calculations and proof-reading of the manuscript; and to Mary Lou Switzer and Cogan Advertising for report reproduction.

ABSTRACT

General harmonic solutions have been found for the camber problem of a ducted propeller with finite blade number in uniform motion at zero incidence. The fluid is assumed inviscid and incompressible. Principal attention is focused on the zeroth harmonic based on a successive iteration of the two-dimensional or sectional Glauert coefficients. In matrix form, the speed of convergence and identification of the limit are studied. Appropriate tables for typical shrouds are provided together with an illustrative example. Both the iteration procedure and direct simultaneous inversion yield solutions for the higher harmonics.

TABLE OF CONTENTS

NOMENCLATURE

a_{m0} , $a_{m\nu}$	Glauert coefficients for A_m , $m > 0$; see Eqs. (3.3)
$\{a_m\}$	column matrix of Glauert coefficients for A_m , $m > 0$
$\{a_{\Gamma,\Gamma'}\}$	column matrix of coefficients of cosine expansion in ϕ of $(A_{\Gamma m} + A_{\Gamma' m})$; see Eqs. (3.9)
A_m	chordwise variation of sine component of mNth harmonic of γ ; see Eqs. (1.3)
$A_{\Gamma m}$	chordwise variation of radial velocity induced on shroud by sine component of mNth harmonic of bound blade vortices; see Eqs. (1.11)
$A_{\Gamma' m}$	chordwise variation of radial velocity induced on shroud by sine component of mNth harmonic of shed blade vortices; see Eqs. (1.11)
b_{m0} , $b_{m\nu}$	Glauert coefficients for B_m , $m > 0$; see Eqs. (3.3)
$\{b_m\}$	column matrix of Glauert coefficients B_m , $m > 0$
$\{b_{\Gamma'}\}$	column matrix of coefficients of cosine expansion in ϕ of $B_{\Gamma' m}$, $m > 0$; see Eqs. (3.9)
B_m	chordwise variation of cosine component of mNth harmonic of γ ; see Eqs. (1.3)

$B_{\Gamma' m}$	chordwise variation of radial velocity induced on shroud by cosine component of mNth harmonic of shed blade vortices; see Eqs. (1.11)
c	shroud chord; see Fig. 1.1
$c_{00}^{(j)}$, $c_{0\nu}^{(j)}$	jth iterate of Glauert coefficients for C_0 , j = 0, 1, 2, ... ; see Eq. (2.5)
$\bar{c}_p$]	net average pressure on shroud, positive radially outward; see Eq. (2.35)
$\{c_0\}$	column matrix of Glauert coefficients of C_0
$\{c_0^{(j)}\}$	column matrix of jth iterate of Glauert coefficients for C_0 , j = 0, 1, 2 ... ; see Eq. (2.20)
c_m	chordwise variation of mNth complex Fourier harmonic of γ ; see Eq. (1.2)
$c_0^{(j)}$	jth iterate of C_0 ; see Eq. (2.4)
g_{mN} , h_{mN}	Fourier integrals arising from shed vorticity; see Eqs. (1.12)
i	$\sqrt{-1}$ and dummy summation index
$\underline{i}_r$	unit vector in r-direction; see Fig. 1.1
I_A , I_B	"particle displacements" for higher harmonic equations in decoupled form

$[I]$	integral matrix operator for singular part of K'_m , identified as infinite unit matrix; see Eqs. (3.5)
j	iteration number and dummy summation index
J	propeller advance ratio, $U/\Omega R_p$
$[J]$	integral matrix operator for singular part of K_m ; see Eqs. (3.7) and (3.8)
k	dummy summation index
K_m	kernel function of final governing equations - for m = 0 only K'_0 appears; see Eqs. (1.7) and (1.14)
$\tilde{\tilde{K}}_m$	regular part of K_m ; see Eqs. (1.9) and (3.4)
$\tilde{\tilde{K}}'_m$	regular part of K'_m , equal to $(\tilde{\tilde{K}}_m)'$
ℓ	dummy summation index
m	harmonic solution index, generally m = 0, 1, 2 ...
$[M]$	matrix of eigenvectors of $[P]$; see Eq. (2.24)
N	number of blades
$[O_K]$	$([J] - [O])$
$[O_{K'}]$	$([I] - [P])$

$P_{k,\ell}$	Fourier coefficients for expansion of $\tilde{\bar{K}}'_m$; for zeroth harmonic $p_{k,\ell}(\lambda)$; see Eq. (2.7)
P_A , P_B	propeller "forcing functions" for higher harmonic equations in decoupled form; see Eqs. (3.1)
$P_{k,\ell}$	elements of [P] , identified as "curvature coefficients" for m = 0 ; see Eqs. (2.10) and (2.18)
[P]	integral matrix operator for regular part of K'_m ; see Eqs. (2.21) and (3.5)
q_i	total induced velocity; see Eq. (1.1)
$Q_{n-\frac{1}{2}}(\tilde{\omega})$	Legendre function of second kind and half order
[Q]	integral matrix operator for regular part of K_m ; see Eqs. (3.7)
$\hat{r}$	r/R_p
R	mean shroud radius at propeller plane; see Fig. 1.1
R_p	propeller tip radius; see Fig. 1.1
S_{mN}	$(Q_{mN+\frac{1}{2}} + Q_{mN-3/2})$
U	forward flight speed; see Fig. 1.1
x,r,θ	cylindrical coordinates fixed in propeller; see Fig. 1.1

x_p	position of propeller plane measured downstream from shroud midchord; see Fig. 1.1
x_s, r_s, θ_s	cylindrical coordinates for point on shroud surface
x_v, r_v, θ_v	cylindrical coordinates for position of vortex element
$\bar{x}$, ...	x/R , ...
$\alpha_{n,\kappa}$, $\beta_{n,\kappa}$	coefficients of small argument expansion of $Q_{n-\frac{1}{2}}(\varpi)$; see Eq. (1.8)
γ	strength of bound shroud vortices; see Fig. 1.1
Γ	strength of bound blade vortex; see Fig. 1.1
$\bar{\Gamma}$	$\Gamma/R_p U$
$\Delta\bar{x}_v$	$(\bar{x}_s - \bar{x}_v)$
$\Delta\bar{x}_p$	$(\bar{x}_s - \bar{x}_p)$
$\Delta\bar{x}_{p\tau}$	$(\bar{x}_s - \bar{x}_p - U\tau/R)$
ϵ	local chordwise shroud slope or camber; see Fig. 1.1
ϵ_e	effective shroud camber

κ	dummy summation index
λ	shroud chord to diameter ratio, $c/2R$
λ_0 , λ_1 , ...	eigenvalues of $[P]$, $\lvert\lambda_0\rvert \geq \lvert\lambda_1\rvert \geq \ldots$; see Eq. (2.29)
$\lambda_0^{(1)}$, ...	successive approximations to λ_0 , ... ; see Eqs. (2.30)
$[\Lambda]$	diagonal matrix with elements λ_0 , λ_1 , λ_2 ... ; see Eq. (2.25)
μ	ratio of propeller tip to mean shroud radius, R_p/R
ν	summation index for Glauert series, $\nu = 1, 2, 3 \ldots$
$\tilde{\omega}$	argument of Legendre function
$\tilde{\omega}_1$	$(1 + \Delta\bar{x}_v^2/2)$
$\tilde{\omega}_3$	$[1 + [\Delta\bar{x}_p^2 + (1-\bar{r}_v)^2] / 2\bar{r}_v]$
$\tilde{\omega}_4$	$[1 + [\Delta\bar{x}_{p\tau}^2 + (1-\bar{r}_v)^2] / 2\bar{r}_v]$
σ	"natural frequency" for higher harmonic equations in decoupled form, $mN/J\mu$
τ	dummy time variable
$\bar{\tau}$	$\Omega\tau$

ϕ	Glauert variable, $\bar{x} = -\lambda \cos \phi$; see Fig. 2.1
$\{\phi_s\}$	column matrix of camber elements for two-dimensional airfoil with unit Glauert coefficients; see Eq. (3.6)
Ω	angular rotational speed of propeller; see Fig. 1.1
$(\ )'$	denotes total differentiation with respect to indicated argument
$\{\ \}^T$	transpose of column matrix or row matrix
$[\ ]^{-1}$	inverse square matrix

GENERAL HARMONIC SOLUTIONS FOR THE DUCTED PROPELLER

INTRODUCTION

In an effort to achieve a general understanding of the ducted propeller, we have previously formulated a three-dimensional theory[1] for the forward flight regime at zero angle of attack. The appropriate mathematical model was based on the classical concepts of vortex propeller theory for finite blading and of lifting surface theory for thin wings in inviscid, incompressible flow.

Primary emphasis was placed on the inverse-direct problem, that is, the determination of the shroud loading for a given blade circulation distribution. By Fourier analysis of the radial component of the propeller velocity field and the bound vortex distribution of the shroud, we reduced the problem for each harmonic to the inversion of a coupled pair of line integrals of the Cauchy type.

The zeroth harmonic corresponds to the representation of the propeller as a generalized actuator disk having the same radial disk loading as its finite bladed counterpart. As such, it determines the average shroud load or the most significant contribution. The higher harmonics give the time-dependent loading on the shroud.

For the zero harmonic, the pair of integral equations degenerates to a single integral equation identical to the equation for an equivalent ring wing with a different effective camber in a uniform flow. The higher harmonics may also be decoupled into a similar form, but with a different kernel because of the swirl of the shroud shed vortices. Since J. Weissinger[2] had formulated the exact solutions to both of these equations, the solutions were left at that time implicitly in terms of his results.

The objective of the present investigation is to obtain explicit solutions. In particular, it is desirable to find the effects of the blade number and loading, the advance ratio, the position of the propeller plane, the tip clearance and the shroud chord to diameter ratio in reasonably simple terms. Except for the influence of the chord to diameter ratio, this is possible for the zeroth harmonic by a study of the effective camber. As the chord to diameter ratio appears in the limits of the integral in the integral equation, its effect requires the inversion of the equation. Unlike the two-dimensional thin airfoil problem, the Glauert coefficients of the direct inversion of the ring wing equation are all coupled by an infinite set of linear equations of infinite extent[2]. Therefore, we attempted to achieve a simplification through an iteration of the corresponding two-dimensional, sectional coefficients which are independently determined. The same would be true

for the higher harmonics in light of the similarity of the decoupled form.

Here we have set forth the iteration procedure in detail, as well as an alternative method for the higher harmonics. Chapter One outlines a brief review of the development of the underlying theory[1] and presents a general discussion of the basic equations to be solved. In Chapter Two, the solution by iteration is found for the zeroth harmonic. Any desired order of iteration is carried out in an explicit form, and in turn, is expressed as the expansion of a single matrix operator of infinite order. This permits the evaluation of the condition and speed of convergence by means of the maximum eigenvalue of the matrix and the identification of the infinite iterate with Weissinger's solution. A numerical example is given, the calculations being based upon the appropriate included tables of curvature coefficients. These coefficients are related to the coefficients tabulated by the Bureau Technique Zborowski[3], but to check, they are computed independently. Finally, Chapter Three contains the iteration solution for the higher harmonics, a direct solution by simultaneous matrix inversion, and a comparison of the features of these solutions.

CHAPTER ONE

BASIC FORMULATION

1.1 Mathematical Model and Background

We consider a ducted propeller in steady forward flight U at constant rotational speed Ω and zero incidence in an inviscid, incompressible fluid otherwise at rest. The shroud and propeller blades are assumed to be infinitely thin and the hub radius infinitely small. These assumptions, together with the restrictions of small shroud camber, moderate chord to diameter ratio and low disk loading permit the conventional approximations of linearized perturbations.

In a propeller-fixed coordinate system x,r,θ, the incoming stream has a uniform translation U in the positive x-direction and a rotational component Ωr in the positive θ-direction, see Fig. 1.1. The blades are at rest in this system, but the duct is rotating about the propeller axis with the angular speed Ω. However, we may set the duct rotation equal to zero without altering the potential solution since we have limited ourselves to axisymmetric ducts at zero angle of attack[1]. Consequently, the determination of the flow is reduced to a steady problem.

The analysis is formulated by the use of appropriate vortex distributions which satisfy the physical boundary conditions. For the propeller, we have the classical

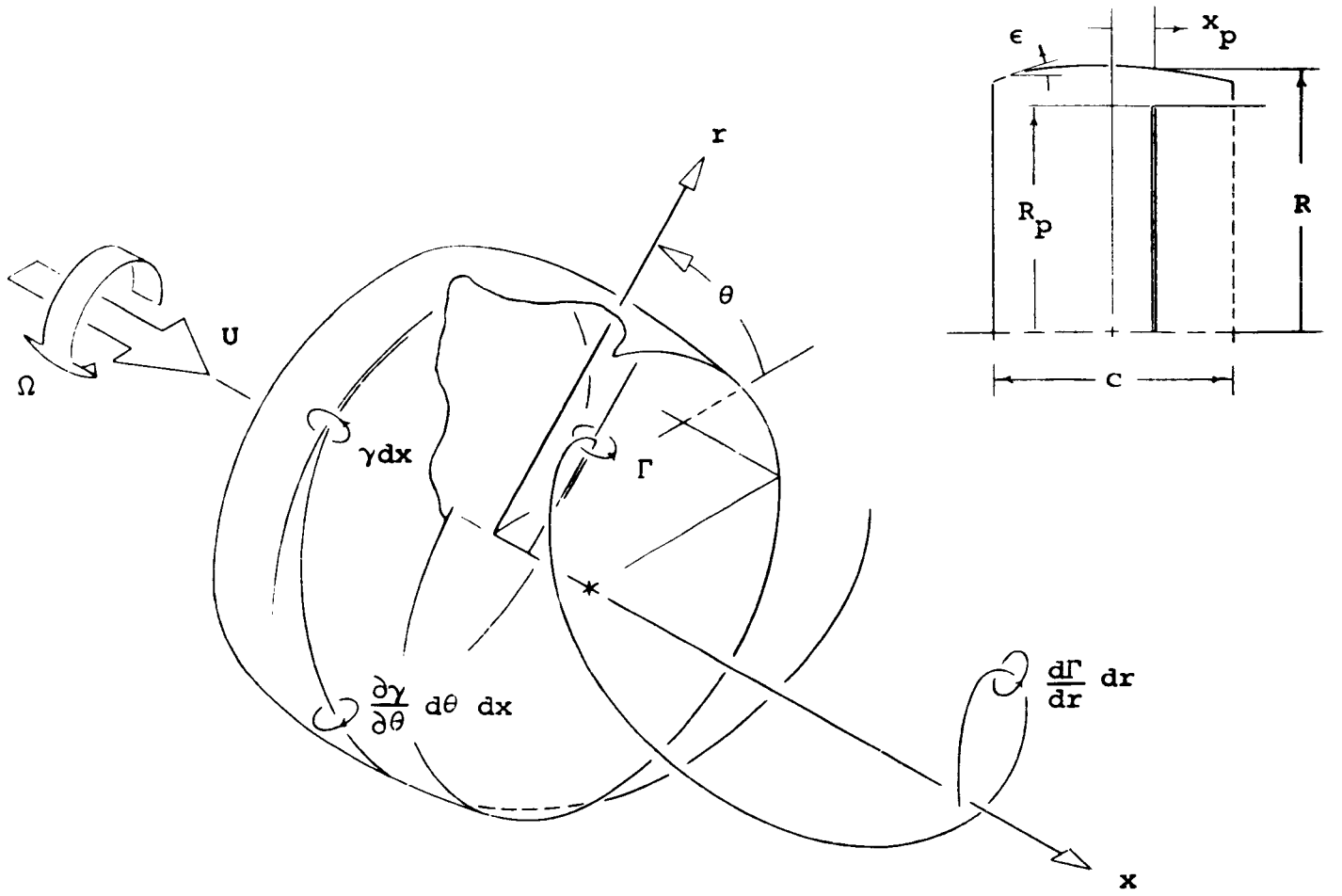

FIGURE 1.1

VORTEX SYSTEM AND GEOMETRY FOR DUCTED PROPELLER CONFIGURATION

representation of a bound radial vortex line of strength $\Gamma(r_v)$ for each blade and the associated helical sheet of strength $-d\Gamma/dr_v$ shed by the line where r_v is the radial distance to any line element. Consistent with our assumptions, the helical path of the shed vortex is determined by the incoming stream. On the other hand, the shroud is composed of bound ring vortices γ which are concentric to the x-axis and have a radius equal to the mean duct radius R. Since the disturbance field introduced by the propeller is not uniform in the angular direction, these bound vortices are accompanied by shed vortex cylinders that are composed of helical vortex elements of strength $-\partial\gamma/\partial\theta_v$. Analogous to the vortices shed from the propeller, their helical pitch is fixed by the incoming stream.

With these vortex distributions, we may determine the basic equation for the shroud vorticity in terms of the propeller circulation. That is, we require that the flow be tangent everywhere on the shroud surface and satisfy the Kutta-Joukowski condition at the trailing edge. With our assumptions, this reduces to a familiar thin airfoil approximation,

$$U\epsilon(x_s) = \underline{q}_i\ (x_s, R, \theta_s)\ \cdot\ \underline{i}_r(\theta_s) \tag{1.1}$$

where ϵ is the local inclination angle of the shroud surface to the x-axis; $\underline{q}_i$ is the sum of the velocities induced

by the four vortex distributions on the mean shroud surface x_s, R, θ_s ; and $\underline{i}_r$ is the local unit vector in the radial direction. The total induced velocity may be determined by means of the Biot-Savart law and Eq. (1.1) reduced to the form of an integral equation for γ with the propeller contributions transposed to the camber term.

1.2 Reduction of the Governing Equation

Generally, the inversion of a surface integral equation is inherently complex. However, in the present case as for the ring wing, the closing of the shroud surface introduces an essential simplification. In particular, $\gamma(x,\theta)$ may be expanded in a complex Fourier series, or

$$\gamma(x,\theta) \equiv U \sum_{m=-\infty}^{\infty} C_m(x)\, e^{imN\theta} \tag{1.2}$$

where C_m vanishes at the shroud trailing edge $x = c/2$ and N is the number of propeller blades of radius R_p . Only the harmonic components mN are necessary because of the periodicity $2\pi/N$ of the propeller field. Since γ is real, the complex coefficients for positive $(+m)$ and negative $(-m)$ integers are complex conjugates, or

$$\begin{aligned} 2C_{-m} &\equiv B_m + iA_m \\ 2C_{+m} &\equiv B_m - iA_m \end{aligned} \tag{1.3}$$

UA_m and UB_m are the real coefficients of the sine and cosine terms respectively of a trigonometric Fourier series for γ over positive m .

For $m = 0$, we note $A_0 = 0$ and $2C_0 = B_0$. This is the zeroth Fourier component of the shroud vorticity in the propeller-fixed coordinates, or equivalently, the time-independent part in the shroud-fixed coordinates. As such, its physical role has been shown to determine the time average difference in shroud inner and outer static pressures.

Substitution of Eq. (1.2) into Eq. (1.1) with the appropriate velocity contributions permits the explicit integration over the angular coordinate and reduces the shroud contributions to their Fourier components in $e^{imN\theta_s}$. At the same time the propeller and shroud camber contributions may be similarly reduced. As a result, the coefficients of these Fourier components may be equated, forming in general, a pair of line integral equations for A_m and B_m . In other words, our original surface integral equation is replaced by a semi-infinite set of coupled, line integral equations for each harmonic[1].

1.3 The Zeroth Harmonic Equation

Since $A_0 \equiv C$, the integral equation for the zeroth harmonic is particularly simple. With $\bar{x}_s \equiv x_s/R$ ... , we have

$$\epsilon_e(\bar{x}_s) = - \int_{-\lambda}^{\lambda} C_C(\bar{x}_v)\, K_C'(\Delta\bar{x}_v)\, d\bar{x}_v \qquad (1.4)$$

where ϵ_e is the "effective" local shroud slope or camber; K_0', the kernel for the zeroth harmonic; $\Delta\bar{x}_v$, the separation of the vortex element and field point $\Delta\bar{x}_v \equiv (\bar{x}_s - \bar{x}_v)$; and λ, the shroud chord to diameter ratio or $\lambda \equiv c/2R$.

The effective camber is composed of the physical shroud camber and the axisymmetric part of the radial field induced by the propeller at the shroud, or

$$\epsilon_e \equiv \epsilon - \tfrac{1}{2} B_{\Gamma' 0} \tag{1.5}$$

The propeller term,

$$B_{\Gamma' 0} = \frac{N}{2\pi^2 J} \int_0^{\mu} \Gamma'(\bar{r}_v)\, Q_{\frac{1}{2}}(\tilde{\omega}_3)\, \bar{r}_v^{\frac{1}{2}}\, d\bar{r}_v$$

$$\tilde{\omega}_3 \equiv 1 + [\Delta\bar{x}_p^2 + (1-\bar{r}_v)^2]/2\bar{r}_v \tag{1.6}$$

depends on the blade number, the advance ratio $J \equiv U/\Omega R_p$, the propeller tip to shroud radius ratio $\mu \equiv R_p/R$, the slope of the blade circulation distribution $\bar{\Gamma}' = d(\Gamma/R_p U)/d\bar{r}_v$, and the propeller plane position $\bar{x}_p$. For convenience, $\bar{\Gamma}$ can be expanded in a suitable sine series and $B_{\Gamma' 0}$ expressed in terms of certain characteristic functions. These functions, involving numerical integration[1] over the Legendre function of second kind and first half order $Q_{\frac{1}{2}}$, have been tabulated over the range of values of $0.0 \leq \bar{x}_p \leq 1.0$ and $0.75 \leq \mu \leq 0.99$.

For $m = 0$, the kernel is simplified by the absence of terms corresponding to helical vortices shed from the shroud. In fact, $-K_0'$ is the radial velocity distribution induced by a ring vortex of positive unit strength and unit radius on a cylinder of which the ring is an element. In terms of $Q_{\frac{1}{2}}$, we have

$$K_0'(\Delta\bar{x}_v) = \frac{1}{2\pi}\Delta\bar{x}_v\, Q_{\frac{1}{2}}'(\tilde{\omega}_1)$$

$$\tilde{\omega}_1 \equiv 1 + \Delta\bar{x}_v^2/2 \qquad (1.7)$$

where as in Γ' , the prime denotes differentiation with respect to the argument of the functions. As we approach the ring, $\Delta\bar{x}_v \to 0$ and $\tilde{\omega}_1 \to 1$. But near unit argument[4,5],

$$Q_{n-\frac{1}{2}}(\tilde{\omega}) = \sum_{\kappa=0}^{\infty} \alpha_{n,\kappa}(\tilde{\omega}-1)^{\kappa} + \ell n(\tilde{\omega}-1)\sum_{\kappa=0}^{\infty}\beta_{n,\kappa}(\tilde{\omega}-1)^{\kappa} \qquad (1.8)$$

For Eq. (1.7) with $n = 1$ we have $\alpha_{1,0} = (5\ell n2 - 4)/2$, $\alpha_{1,1} = (15\ell n2 - 2)/16$, ... and $\beta_{1,0} = -1/2$, $\beta_{1,1} = -3/16$, ... Therefore, the singular part of $-K_0'$ is equal to $1/2\pi\Delta\bar{x}_v$, i.e., in the immediate vicinity of the vortex, the flow field is equivalent to a two-dimensional line vortex tangent to the ring and the integral of Eq. (1.4) must be interpreted as the Cauchy principal value. On the other hand, the regular part of the kernel, say $\tilde{K}_0'$, where

$$\tilde{\tilde{K}}_0' \equiv K_0' + 1/2\pi\Delta\bar{x}_v \tag{1.9}$$

represents the three-dimensional effect of the ring which vanishes as the ring radius become infinite. $\tilde{\tilde{K}}_0'$ behaves as $\Delta\bar{x}_v \ln \Delta\bar{x}_v$ near the vortex, increases to a maximum and then decays monotonically to zero as $\Delta\bar{x}_v \to \infty$. By inspection of Eqs. (1.7) and (1.8), both the singular and regular parts of the kernel are antisymmetric about $\Delta\bar{x}_v = 0$. If we compare Eq. (1.4) with Weissinger's ring wing equation for zero angle of attack, we find[1] that the forms are identical with "$U_0(\eta)$" equal to $-2\pi\tilde{\tilde{K}}_0'$.

1.4 The Higher Harmonic Equations

For m, $J \neq 0$, the integral equations for A_m and B_m are considerably more complex. The essential complications arise from the additional terms introduced by the helical shed vortices which couple the integral equations, or

$$A_{\Gamma m} + A_{\Gamma' m} = \int_{-\lambda}^{\lambda} A_m K_m' \, d\bar{x}_v + \sigma \int_{-\lambda}^{\lambda} B_m K_m \, d\bar{x}_v$$

$$B_{\Gamma' m} = \int_{-\lambda}^{\lambda} B_m K_m' \, d\bar{x}_v - \sigma \int_{-\lambda}^{\lambda} A_m K_m \, d\bar{x}_v \tag{1.10}$$

with $\sigma \equiv mN/J\mu$. The term $UA_{\Gamma m}$ is the coefficient of the mN^{th} harmonic in the Fourier sine expansion of the radial velocity component induced on the duct by the bound radial vortex lines which represent the propeller. $UA_{\Gamma' m}$ and

$UB_{\Gamma' m}$ are the coefficients of the mN^{th} sine and cosine harmonics, respectively, in the Fourier expansion of the radial velocity component induced on the duct by the helical vortices shed from the blades. These terms are given by

$$A_{\Gamma m} = -\frac{\mu mN^2}{2\pi^2}\,\Delta\bar{x}_p \int_0^{\mu} \frac{\bar{\Gamma}}{\bar{r}_v^{3/2}}\, Q_{mN-\frac{1}{2}}\, d\bar{r}_v$$

$$A_{\Gamma' m} = \frac{N}{4\pi^2 J} \int_0^{\mu} \bar{\Gamma}'\, \bar{r}_v^{-\frac{1}{2}}\, h_{mN}\, d\bar{r}_v$$

$$B_{\Gamma' m} = \frac{N}{4\pi^2 J} \int_0^{\mu} \bar{\Gamma}'\, \bar{r}_v^{-\frac{1}{2}}\, (S_{mN} - g_{mN})\, d\bar{r}_v \qquad (1.11)$$

where the argument of $Q_{mN-\frac{1}{2}}$ and S_{mN} is $\tilde{\omega}_3$ of Eq. (1.6), $Q_{mN-\frac{1}{2}}$ is the general Legendre function of second kind and half order, and S_{mN} is the sum of $Q_{mN+\frac{1}{2}}$ and $Q_{mN-3/2}$. The functions g_{mN} and h_{mN} are Fourier integrals defined by

$$\begin{matrix} g_{mN}(\Delta\bar{x}_p, \bar{r}_v) \\ h_{mN}(\Delta\bar{x}_p, \bar{r}_v) \end{matrix} \equiv$$

$$mN \int_0^{\infty} \left[\frac{2J^2\mu^2}{\bar{r}_v} Q_{mN-\frac{1}{2}} + S_{mN}\right] \begin{matrix} (\sin mN\bar{\tau}) \\ (\cos mN\bar{\tau}) \end{matrix} d\bar{\tau} \qquad (1.12)$$

$Q_{mN-\frac{1}{2}}$ and S_{mN} have the argument $\tilde{\omega}_4$ which is equal to $\tilde{\omega}_3$ with $\Delta\bar{x}_p$ replaced by the quantity $\Delta\bar{x}_{p\tau} \equiv (\Delta\bar{x}_p - U\tau/R)$, the $Q_{mN-\frac{1}{2}}$ term arising from the axial elements of the helical

vortices and the S_{mN} term, from the tangential. τ is a variable representing the time for a vortex element, convected by the free stream, to travel from the point of shedding to its position on the helix and $\bar{\tau} \equiv \Omega\tau$. For μ , and so $\bar{r}_v$, less than unity, there is no question about the behavior of g_{mN} and h_{mN} . When μ is equal to unity, Eq. (1.8) assures that the singular integrand is integrable, and the asymptotic form[5] of the Legendre function, or

$$Q_{n-\frac{1}{2}}(\tilde{\omega}) = \frac{\pi}{2^{3n+\frac{1}{2}}} \frac{(2n)!}{(n!)^2} \frac{1}{\tilde{\omega}^{n+\frac{1}{2}}} + \ldots \tag{1.13}$$

that it is convergent far downstream.

The kernel function may also be defined in terms of S_{mN} and g_{mN} . We find,

$$K_m(\Delta\bar{x}_v) = \frac{1}{4\pi} [S_{mN}(\tilde{\omega}_1) - g_{mN}(\Delta\bar{x}_v, 1)] \tag{1.14}$$

where g_{mN} has been evaluated at $\bar{r}_v = 1$ or on the shroud.

To understand the form of Eqs. (1.10), further description of the kernel function K_m is necessary. The term $-\Delta\bar{x}_v S'_{mN}/4\pi$ is identified as the mN^{th} harmonic of the radial velocity induced on the shroud by the shroud bound vortices in non-dimensional form. In other words, the radial velocity of a ring vortex of strength $UA_m \sin mN\theta_v dx_v$ is $(UA_m \sin mN\theta_v d\bar{x}_v)$ $(-\Delta\bar{x}_v S'_{mN}/4\pi)$, or "in-phase" with the strength variation.

In the neighborhood of the ring, the vortex again appears as a straight, infinite line vortex tangent to the ring with a strength equal to the local strength, see Eq. (1.8), and the integrals of Eqs. (1.10) are interpreted in the Cauchy principal value sense. As the axial separation is increased, the induced radial velocity decays, the asymptotic behavior determined by Eq. (1.13).

The other term in K_m' and the terms of K_m constitute the influence of the shroud shed vortices. Examination of these terms reveals that the term $S_{mN}/4\pi$ contains the "end effect" of the semi-infinite cylinder of helical vortices shed from our bound ring vortex at $\Delta\bar{x}_v = 0$. In other words, as we approach the ring, its shed vortices form an effective planar sheet of vortices which have a constant strength equal to the rate of change of the local bound vortex strength and inclined at the angle having the tangent $1/J\mu$ to the x-axis. This sheet is equivalent to the superposition of two semi-infinite sheets of vortices, parallel and perpendicular to the x-axis. But by symmetry the parallel vortices cannot contribute to the "normal" or radial velocity since the contributions from either side are equal and opposite, see Fig. 1.2. On the other hand, the vortices perpendicular to the x-axis form an unbalanced sheet and integrate to a logarithmic singularity given by $S_{mN}/4\pi$, see Eq. (1.8).

The remaining terms $g_{mN}(\Delta\bar{x}_v,1)$ and $g'_{mN}(\Delta\bar{x}_v,1)$ involved in Eqs. (1.10) are both regular, the behavior of

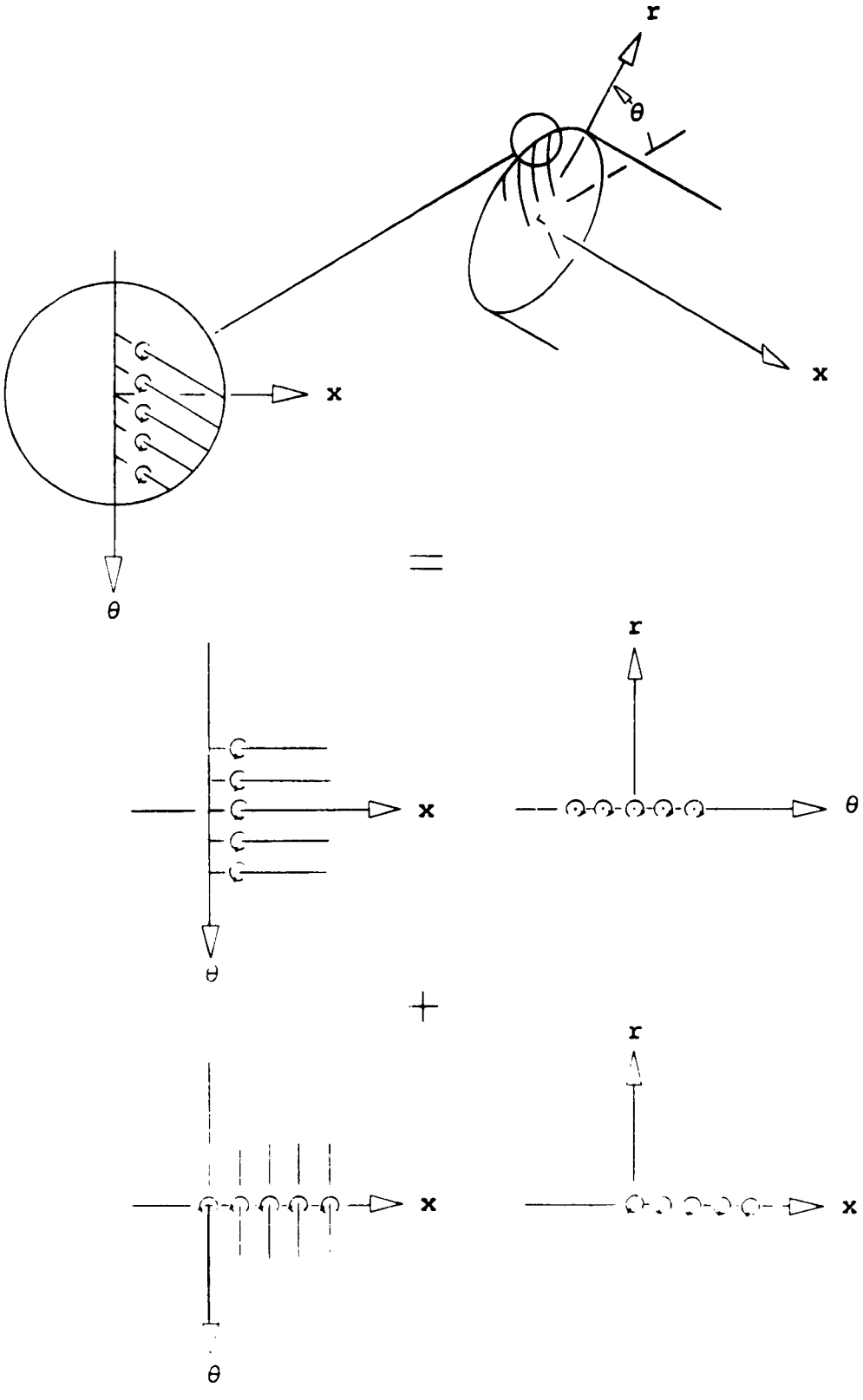

FIGURE 1.2

DECOMPOSITION OF THE LOCAL SHED VORTEX SHEET

$g_{mN}(\Delta\bar{x}_v,1)$ following from our previous discussion for the propeller for zero tip clearance. It may be shown that

$$g'_{mN}(\Delta\bar{x}_v,1) = \frac{mN}{J\mu} h_{mN}(\Delta\bar{x}_v,1) \tag{1.15}$$

and consequently, from Eqs. (1.8), (1.12) and (1.13), $g'_{mN}(\Delta\bar{x}_v,1)$ is regular. The logarithmic singularities of the integrands of both $g_{mN}(\Delta\bar{x}_v,1)$ and $h_{mN}(\Delta\bar{x}_v,1)$ may be interpreted analogous to $S_{mN}/4\pi$. That is, for a field point downstream of a vortex ring at $\bar{x}_v$, the shed vortices from the ring locally appear as an infinite planar surface of constant strength vortices inclined to the x-axis. Only this time, by symmetry, both the contributions to the "normal" or radial velocity from the component sheets parallel and perpendicular to the x-axis cancel.

The kernel function K_m or, more important as we will see, its derivative K'_m with g'_{mN} given by Eq. (1.15) has not been evaluated in general in closed form. For the special case, however, of infinite advance ratio, the integral equations decouple, the terms in K_m vanishing. The K'_m terms remain and h_{mN} reduces to simply an integral over $Q_{mN-\frac{1}{2}}$, or a cylinder of semi-infinite straight line vortices parallel to the x-axis. This may be integrated explicitly[1] and yields the result,

$$\lim_{J\to\infty} K'_m = -\frac{U_m}{2\pi} - \frac{1}{2\pi\Delta\bar{x}_v} - \frac{mN}{4} \tag{1.16}$$

where "U_m" is the function introduced by J. Weissinger in his ring wing theory. It is a regular function, increasing with a logarithmic slope from zero at the origin to an asymptotic value of $\pi mN/2$ as $\Delta\bar{x}_v \to \infty$ for $m > 0$. As $m \to \infty$, $U_m/\frac{1}{2}\pi mN$ approaches the general form of a unit step function $1(\Delta\bar{x}_v)$.

CHAPTER TWO

DETERMINATION OF THE NET AVERAGE DUCT LOAD

2.1 General Considerations

If we neglect the regular part of the kernel for the zeroth harmonic, Eq. (1.4) reduces by means of Eq. (1.9) to the integral equation of the classical two-dimensional thin airfoil problem. To solve, we introduce a new axial coordinate ϕ such that

$$\bar{x} = - \lambda \cos \phi \tag{2.1}$$

where $0 \leq \phi \leq \pi$, see Fig. 2.1. Expressing the vortex distribution $c_0(\bar{x})$ in a Glauert series, we can then invert the integral equation and obtain a solution explicitly in terms of the Fourier cosine coefficients of the effective camber distribution.

As we have pointed out, $\tilde{\tilde{K}}_0'$ represents the three-dimensional effect of the shroud. Thus, we can consider this contribution as a correction to be combined with the effective camber, permitting an iteration solution of Eq. (1.4) in the form of the Glauert series. That is, we may write from Eq. (2.1)

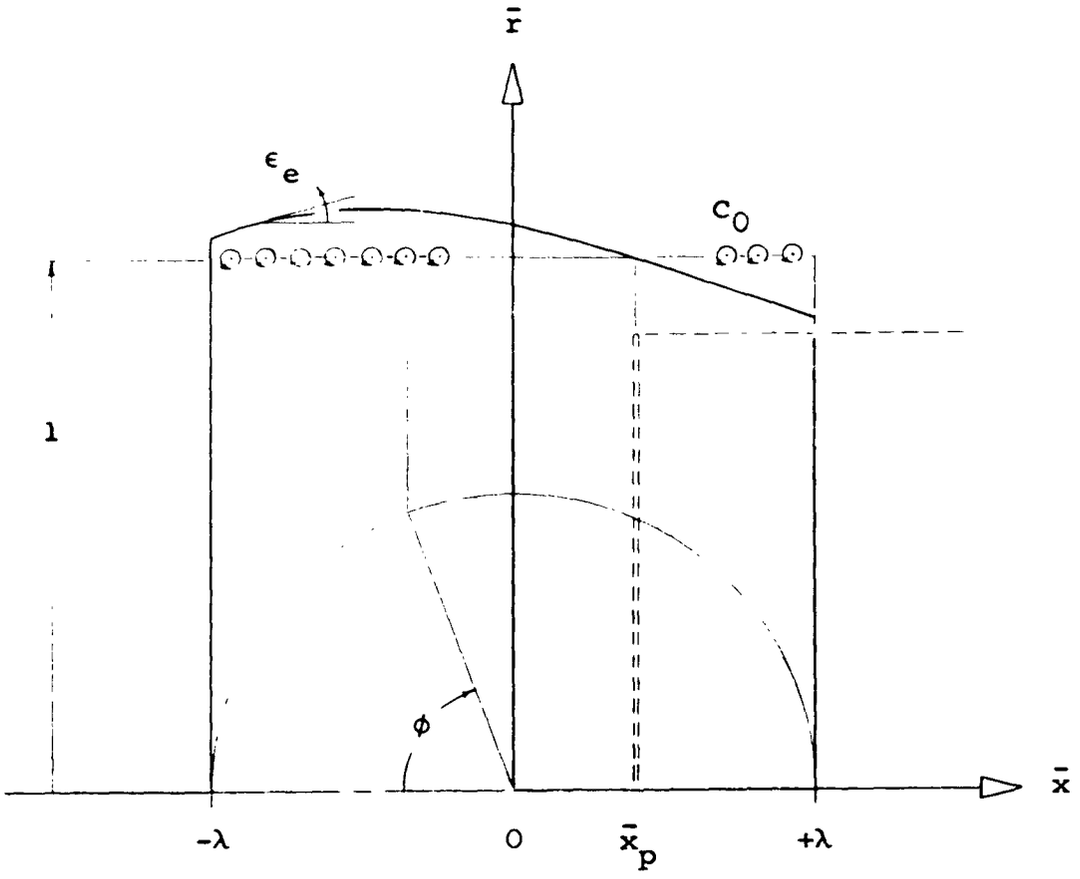

FIGURE 2.1

TRANSFORMATION TO GLAUERT VARIABLE FOR EQUIVALENT RING AIRFOIL

$$\epsilon_e + \lambda \int_0^{\pi} C_0 \, \tilde{\tilde{K}}_0' \sin \phi_v \, d\phi_v$$

$$= \frac{1}{2\pi} \int_0^{\pi} \frac{C_0 \sin \phi_v}{\cos \phi_v - \cos \phi_s} \, d\phi_v \tag{2.2}$$

where the regular part of the kernel is

$$\tilde{\tilde{K}}_0' = \tilde{\tilde{K}}_0'(\lambda \cos \phi_v - \lambda \cos \phi_s) \tag{2.3}$$

and C_0 is implicitly a function of ϕ_v. Then, if we set C_0 equal to zero on the left hand side of Eq. (2.2), we can find a "zeroth" approximation from the two-dimensional theory. Inserting this distribution back into the left hand side, we determine a first approximation which includes a correction due to the surface curvature. Subsequently, the procedure may be repeated. In the limit, it will converge to the exact solution of Eq. (1.4), or

$$C_0 = \lim_{j \to \infty} C_0^{(j)} \tag{2.4}$$

where

$$C_0^{(j)} = C_{00}^{(j)} \frac{1 + \cos \phi}{\sin \phi} + \sum_{\nu=1}^{\infty} C_{0\nu}^{(j)} \sin \nu\phi \tag{2.5}$$

and the superscript (j) denotes the j^{th} iteration, $j = 0, 1, 2, \ldots$. Such a solution possesses the familiar

leading and trailing edge behavior of an infinitely thin, two-dimensional airfoil, i.e., a square-root singularity at the leading edge and vanishing perturbational velocity at the trailing edge.

2.2 Expansion of the Kernel Function

To facilitate the iteration we expand $\tilde{\tilde{K}}_0'$ in the square $0 \leq \phi_s \leq \pi$ and $0 \leq \phi_v \leq \pi$ as

$$\tilde{\tilde{K}}_0' = \sum_{k=0}^{\infty} \sum_{\ell=0}^{\infty} p_{k,\ell}(\lambda) \cos k\phi_s \cos \ell\phi_v \tag{2.6}$$

The Fourier coefficients $p_{k,\ell}(\lambda)$ from orthogonality are

$$p_{k,\ell} = \frac{4}{\pi^2} \int_0^{\pi} \int_0^{\pi} \cos k\phi_s \cos \ell\phi_v \, \tilde{\tilde{K}}_0' \, d\phi_v \, d\phi_s \tag{2.7}$$

for k , $\ell \neq 0$; $p_{k,0}$ and $p_{0,\ell}$ are one-half and $p_{0,0}$ one-quarter of these values. Since $\tilde{\tilde{K}}_0'$ is an odd function in $\Delta\bar{x}_v$, see Eqs. (1.7) and (1.9), we may interchange ϕ_s and ϕ_v in Eqs. (2.3) and (2.7) and find,

$$p_{k,\ell} = - p_{\ell,k} \tag{2.8}$$

Consequently, $p_{0,0}$, $p_{1,1}$, $p_{2,2}$ ... all identically vanish. In addition, we may replace ϕ_s by $(\pi-\phi_s)$ and ϕ_v by $(\pi-\phi_v)$ in Eq. (2.7) and show that $p_{k,\ell} \equiv 0$ if $(k+\ell)$ is an even integer.

These coefficients may be related to the work of J. Weissinger[2] who expanded an integral over a weighted kernel function instead of the regular part of the kernel. From this integral designated by "f_ν" , we find after comparison of nomenclature,

$$p_{k,\ell} = \frac{1}{\pi^2} b_{\nu,\mu} \tag{2.9}$$

where the "$b_{\nu,\mu}$'s" are the coefficients he used with $\nu = k$ and $\mu = \ell$ for $\nu,\mu \neq 0$ but reduced like the $p_{k,\ell}$'s in Eq. (2.7) for vanishing ν and/or μ . The Bureau Technique Zborowski has tabulated[3] the "$b_{\nu,\mu}$'s" for $\lambda = 0.5,\ 1.0,\ 1.5,$ and 2.0 and $\nu,\mu = 0,\ 1,\ \ldots\ 7$.

Subsequently, we will find that these coefficients as such do not appear, but rather the combinations given by,

$$P_{k,0} \equiv \lambda\pi\ (-p_{k,1} - 2p_{k,0})$$

$$P_{k,1} \equiv \frac{\lambda\pi}{2}\ (p_{k,2} - 2p_{k,0})$$

$$P_{k,2} \equiv \frac{\lambda\pi}{2}\ (p_{k,3} - p_{k,1})$$

$$\vdots$$

$$P_{k,\ell} \equiv \frac{\lambda\pi}{2}\ (p_{k,\ell+1} - p_{k,\ell-1}) \tag{2.10}$$

except for $k = 0$, in which case they are of opposite sign. Their values for $k, \ell = 0, 1, \ldots 7$ have been computed from Eqs. (2.7) and (2.10) by a relaxation procedure[6] carried out until the difference between successive computations is less than ± 0.00001. The results over the range of $\lambda = 0.25$, 0.50, 0.75 and 1.0 are presented in Tables 2.1, 2.2, 2.3 and 2.4 respectively. For $\lambda = 0.50$ and 1.0, they are in general the same as found by means of Eq. (2.9) from the tables of the Bureau Technique Zborowski[3] within a discrepancy of $0(0.001)$ or less, except for a few diagonal terms at the higher values of k and ℓ.

2.3 Iterative Solution

We can now pursue the development of the iterative solution as previously outlined.

First, we reduce Eq. (2.2) to the two-dimensional form for the zeroth approximation $c_0^{(0)}$, or

$$\epsilon_e = \frac{1}{2\pi} \int_0^{\pi} \frac{c_0^{(0)} \sin \phi_v}{\cos \phi_v - \cos \phi_s} \, d\phi_v \tag{2.11}$$

The solution is given by the classical form of H. Glauert[7], or Eq. (2.5) with $j = 0$. To determine the coefficients, $c_0^{(0)}$ is substituted into Eq. (2.11). After suitable manipulation of the integrand by trigonometric identities, the integration may be carried out term by term by means of the well known relation

TABLE 2.1

CURVATURE COEFFICIENTS $P_{k,\ell}$ FOR $\lambda = 0.25$

k \ ℓ	0	1	2	3	4	5	6
0	0.02683	0	0.01343	0	-0.00001	0	0.00000
1	0.05366	0.02987	0	-0.00304	0	0.00000	0
2	0.00608	0	0.00403	0	-0.00099	0	0.00000
3	-0.00005	-0.00101	0	0.00148	0	-0.00049	0
4	-0.00001	0	-0.00049	0	0.00079	0	-0.00029
5	0.00000	0.00000	0	-0.00029	0	0.00049	0
6	0.00000	0	0.00000	0	-0.00020	0	0.00034

TABLE 2.2

CURVATURE COEFFICIENTS $P_{k,\ell}$ FOR $\lambda = 0.50$

k \ ℓ	0	1	2	3	4	5	6
0	0.07281	0	0.03644	0	-0.00004	0	0.00000
1	0.14561	0.08526	0	-0.01252	0	0.00006	0
2	0.02491	0	0.01655	0	-0.00411	0	0.00002
3	-0.00016	-0.00417	0	0.00609	0	-0.00200	0
4	-0.00013	0	-0.00206	0	0.00318	0	-0.00119
5	0.00000	0.00002	0	-0.00120	0	0.00197	0
6	0.00000	0	0.00001	0	-0.00078	0	0.00134

TABLE 2.3

CURVATURE COEFFICIENTS $P_{k,\ell}$ FOR $\lambda = 0.75$

k \ ℓ	0	1	2	3	4	5	6
0	0.11925	0	0.05945	0	0.00019	0	-0.00001
1	0.23849	0.14668	0	-0.02765	0	0.00021	0
2	0.05488	0	0.03702	0	-0.00965	0	0.00007
3	0.00071	-0.00922	0	0.01418	0	-0.00463	0
4	-0.00042	0	-0.00482	0	0.00732	0	-0.00272
5	-0.00005	0.00005	0	-0.00278	0	0.00450	0
6	0.00000	0	0.00002	0	-0.00181	0	0.00306

TABLE 2.4

CURVATURE COEFFICIENTS $P_{k,\ell}$ FOR $\lambda = 1.00$

k \ ℓ	0	1	2	3	4	5	6
0	0.16016	0	0.07907	0	0.00107	0	-0.00006
1	0.32032	0.20609	0	-0.04629	0	0.00035	0
2	0.09186	0	0.06338	0	-0.01766	0	0.00020
3	0.00402	-0.01544	0	0.02592	0	-0.00855	0
4	-0.000[illegible]	0	-0.00883	0	0.01338	0	-0.00495
5	-0.00025	0.00008	0	-0.00512	0	0.00814	0
6	-0.00003	0	0.00006	0	-0.00330	0	0.00550

$$\int_0^{\pi} \frac{\cos \kappa\phi_v}{\cos \phi_v - \cos \phi_s} \, d\phi_v = \frac{\sin \kappa\phi_s}{\sin \phi_s} \tag{2.12}$$

for $\kappa = 0, 1, 2, \ldots$. As a result, the contribution for the singular component of the vortex distribution is constant; i.e., the uniform induced velocity for a flat plate in two-dimensional flow. The contribution for each sine harmonic is a corresponding cosine harmonic. Or,

$$\epsilon_e = \frac{1}{2} c_{00}^{(0)} - \frac{1}{2} \sum_{\nu=1}^{\infty} c_{0\nu}^{(0)} \cos \nu\phi_s \tag{2.13}$$

By orthogonality, then,

$$c_{00}^{(0)} = \frac{2}{\pi} \int_0^{\pi} \epsilon_e \, d\phi_s$$

$$c_{0\nu}^{(0)} = -\frac{4}{\pi} \int_0^{\pi} \epsilon_e \cos \nu\phi_s \, d\phi_s \tag{2.14}$$

for $\nu = 1, 2, \ldots$. Eq. (2.14) together with Eq. (2.5) with $j = 0$ provides the zeroth approximation with ϵ_e as a function of ϕ_s given by Eqs. (1.5), (1.6) and (2.1). Note that the signs of Eq. (2.13) are reversed from the usual two-dimensional airfoil result[7] because we have defined the positive sense of the bound vortices according to the right hand screw rule, see Fig. 2.1.

Next, we replace c_0 by $c_0^{(0)}$ in the left hand side of Eq. (2.2) and obtain an equation for the first approximation $c_0^{(1)}$ to the bound vortex distribution. This equation is the same as Eq. (2.11) except that the effective camber is changed by the additional curvature term. To solve, we substitute Eq. (2.5) with $j = 1$ and proceed as before. The right hand side reduces correspondingly to the form of the right hand side of Eq. (2.13) with the new coefficients $c_{00}^{(1)}$ and $c_{0\nu}^{(0)}$. For the left hand side, we use Eq. (2.13) for ϵ_e and the expansion of Eq. (2.6) for $\tilde{\tilde{K}}_0'$. The integration over $\tilde{\tilde{K}}_0'$ is carried out by means of the integrals,

$$\int_0^\pi \cos \ell\phi_v \, d\phi_v = \begin{cases} \pi , & \ell = 0 \\ 0 , & \ell = 1, 2, 3, \ldots \end{cases} \tag{2.15}$$

$$\int_0^\pi \cos \phi_v \cos \ell\phi_v \, d\phi_v = \begin{cases} \pi/2 , & \ell = 1 \\ 0 , & \ell = 0, 2, 3, 4, \ldots \end{cases} \tag{2.16}$$

$$\int_0^\pi \sin \nu\phi_v \cos \ell\phi_v \sin \phi_v \, d\phi_v = \begin{cases} \pi/2 , & \ell = \nu - 1 = 0 \\ \pi/4 , & \ell = \nu - 1 > 0 \\ 0 , & \ell \neq \nu \pm 1 \\ -\pi/4 , & \ell = \nu + 1 \end{cases} \tag{2.17}$$

and yields in turn a cosine series. Equating coefficients of like terms, we have

$$c_{00}^{(1)} = c_{00}^{(0)} + P_{0,0}\, c_{00}^{(0)} + P_{0,1}\, c_{01}^{(0)} + \cdots$$

$$c_{01}^{(1)} = c_{01}^{(0)} + P_{1,0}\, c_{00}^{(0)} + P_{1,1}\, c_{01}^{(0)} + \cdots$$

$$\vdots \qquad (2.18)$$

Eqs. (2.18) reveal that the first approximation to any coefficient of our bound vortex distribution for the zeroth shroud harmonic is equal to the two-dimensional value of the coefficient plus a correction. The correction is determined from all the coefficients of the zeroth approximation weighted by the curvature coefficients $P_{k,\ell}$. In other words, each of the basic vortex distributions which represent the effective camber in the two-dimensional case induce an additional camber when introduced as a three-dimensional distribution.

This process may be repeated successively. Since only the superscript varies, we have the expressions,

$$c_{00}^{(j)} = c_{00}^{(0)} + P_{0,0}\, c_{00}^{(j-1)} + P_{0,1}\, c_{01}^{(j-1)} + \cdots$$

$$c_{01}^{(j)} = c_{00}^{(0)} + P_{1,0}\, c_{00}^{(j-1)} + P_{1,1}\, c_{01}^{(j-1)} + \cdots$$

$$\vdots \qquad (2.19)$$

for the j^{th} approximation in recursion form. Eq. (2.19) together with Eqs. (2.4) and (2.5) then constitute the exact solution for C_0 if the limit exists.

For a symmetric effective airfoil or $\epsilon_e(-x) = \epsilon_e(x)$, we have $c_{00}^{(0)}$, $c_{02}^{(0)}$, $c_{04}^{(0)}$ ... $\equiv 0$ from Eqs. (2.14). But $P_{0,1}$, $P_{0,3}$, $P_{0,5}$ ... are identically zero as well as $P_{2,1}$, $P_{2,3}$, $P_{2,5}$ ... and $P_{4,1}$, $P_{4,3}$, $P_{4,5}$ ...and so forth, see Eqs. (2.10). From Eqs. (2.19), then, $c_{00}^{(j)}$, $c_{02}^{(j)}$, $c_{04}^{(j)}$ ... $\equiv 0$ for any value of j, reducing the Glauert series of Eq. (2.5) to only the terms for $\nu = 1, 3, 5 \ldots$. Therefore, the net loading for the zeroth harmonic would be symmetric about the midchord and zero at both the leading and trailing edges as required by consideration of the corresponding solution for the equivalent ring airfoil in reverse flow.

2.4 Convergence of the Iteration

From physical considerations the convergence of the solution depends on λ. If the shroud diameter is infinitely large compared to the shroud chord, $P_{k,\ell} \equiv 0$ and $c_0^{(j)}$ "converges" to the exact, two-dimensional solution in a single step. As λ increases, the three-dimensional effect of the shroud increases, reducing the domination of the Cauchy integral in Eq. (2.2). The speed of convergence is expected to diminish accordingly and, in fact, to vanish as $\lambda \to \infty$.

To examine this, we use matrix operations. We define the infinite column matrix of the Glauert coefficients,

$$\{c_0^{(j)}\} \equiv \begin{Bmatrix} c_{00}^{(j)} \\ c_{01}^{(j)} \\ c_{02}^{(j)} \\ \vdots \end{Bmatrix} \tag{2.20}$$

and the infinite square matrix of the curvature coefficients

$$[P] \equiv \begin{bmatrix} P_{0,0} & P_{0,1} & P_{0,2} & \cdots \\ P_{1,0} & P_{1,1} & P_{1,2} & \\ P_{2,0} & P_{2,1} & P_{2,2} & \\ \vdots & & & \end{bmatrix} \tag{2.21}$$

With Eqs. (2.20) and (2.21), Eqs. (2.19) become

$$\{c_0^{(j)}\} = \{c_0^{(0)}\} + [P]\{c_0^{(j-1)}\} \tag{2.22}$$

If we apply Eq. (2.22) to the first and subsequent approximations and use the unit matrix $[I]$ of infinite order, we have

$$\{c_0^{(j)}\} = ([I] + [P] + [P]^2 + \ldots [P]^j)\{c_0^{(0)}\} \tag{2.23}$$

That is, each iteration corresponds to a successive application of the matrix of the curvature coefficients. Hence, the iteration will converge if and only if the limit of the sum of these operations as $j \to \infty$, or Neumann series, exists[8].

Letting $[M]$ be a matrix with columns composed of the eigenvectors of $[P]$, we have

$$[P] = [M]\,[\Lambda]\,[M]^{-1} \tag{2.24}$$

where $[M]^{-1}$ denotes the inverse of $[M]$ and $[\Lambda]$ is a diagonal matrix,

$$[\Lambda] \equiv \begin{bmatrix} \lambda_0 & 0 & 0 & \cdots \\ 0 & \lambda_1 & 0 & \\ 0 & 0 & \lambda_2 & \\ \vdots & & & \end{bmatrix} \tag{2.25}$$

of the associated eigenvalues of $[P]$ or $\lambda_0, \lambda_1, \lambda_2 \ldots$. These elements are numbered such that $|\lambda_0| \geq |\lambda_1| \geq |\lambda_2| \ldots$, where the eigenvalue in $[\Lambda]$ is in the same column as its corresponding eigenvector in $[P]$.

By means of Eq. (2.24), we may express the repeated

operation of $[P]$ on itself by,

$$[P]^j = [M]\,[\Lambda]^j\,[M]^{-1} \tag{2.26}$$

Substitution of Eq. (2.26) into the j^{th} term of Eq. (2.23) then yields,

$$\{c_0^{(j)}\} = [M]\,([I] + [\Lambda] + [\Lambda]^2 + \ldots + [\Lambda]^j)\,[M]^{-1}\,\{c_0^{(0)}\} \tag{2.27}$$

with $([I] + [\Lambda] + [\Lambda]^2 + \ldots [\Lambda]^j)$ equal to,

$$\begin{bmatrix} (1+\lambda_0+\lambda_0^2+\ldots\lambda_0^j) & 0 & 0 & \ldots \\ 0 & (1+\lambda_1+\lambda_1^2+\ldots\lambda_1^j) & 0 & \\ 0 & 0 & (1+\lambda_2^2+\lambda_2^3+\ldots\lambda_2^j) & \\ \vdots & & & \end{bmatrix}$$

By inspection, the limit exists if the limiting elements $(1+\lambda_0+\lambda_0^2+\ldots)$, $(1+\lambda_1+\lambda_1^2+\ldots)$, ... exist, or equivalently if

$$|\lambda_0| < 1 \tag{2.28}$$

since λ_0 is the greatest eigenvalue in absolute magnitude. This inequality constitutes a criterion for, and assures the convergence of, the iteration process.

In principle, we can determine λ_0 for each chord to diameter ratio exactly from the secular equation of [P] or

$$0 = | [P] - \lambda_{0,1,2\ldots} [I] | \tag{2.29}$$

In practice, however, we generally have to resort to an approximate calculation. One method is to assume a trial eigenvector of unit elements and operate with [P] successively. If we choose a corresponding eigenvalue $\lambda_0^{(0)}$ of unity and normalize the leading element at each step, we have for the first $\lambda_0^{(1)}$ and subsequent approximations,

$$\lambda_0^{(1)} = (\sum_i P_{0,i}) / \lambda_0^{(0)}$$

$$\lambda_0^{(2)} = (\sum_j \sum_i P_{0,j} P_{j,i}) / \lambda_0^{(1)}$$

$$\lambda_0^{(3)} = (\sum_k \sum_j \sum_i P_{0,k} P_{k,j} P_{j,i}) / \lambda_0^{(2)}$$

$$\vdots \tag{2.30}$$

We have computed λ_0 for $\lambda = 0.25, 0.50, 0.75$ and 1.00 from Eqs. (2.30) and Tables 2.1, 2.2, 2.3 and 2.4 respectively.

The results are given in Fig. 2.2 and Table 2.5 and overlap λ_0 for $\lambda = 0.5, 1.0, 1.5,$ and 2.0 computed from the BTZ data[3].

Immediately we see from Eq. (2.38) that our solution converges, at least for $0 \leq \lambda \leq 2$. We see also that the speed of convergence decreases as anticipated. That is, from Eq. (2.27) λ_0^j determines the accuracy of the j^{th} iteration. Since λ_0 increases with increasing λ , the number of iterations for convergence to a prescribed accuracy increases.

We have no numerical data beyond a chord to diameter ratio of two. On the other hand, the radial flow induced by a vortex element of a vortex ring through a point on the shroud can not be as "large" as the "infinite" contribution of the element at the point itself unless the shroud radius is zero. Consequently, the extremum eigenvalue should continue to increase, approaching unity asymptotically as $\lambda \to \infty$. We will see later that $\lambda_0 \neq 1$. Physically, it can not return to zero.

2.5 Example

To illustrate the iteration procedure we have computed the net shroud pressure distribution of the average load for a particular ducted propeller with an effective conical camber.

The distribution selected for the propeller circulation is the typical distribution which was previously used[1],

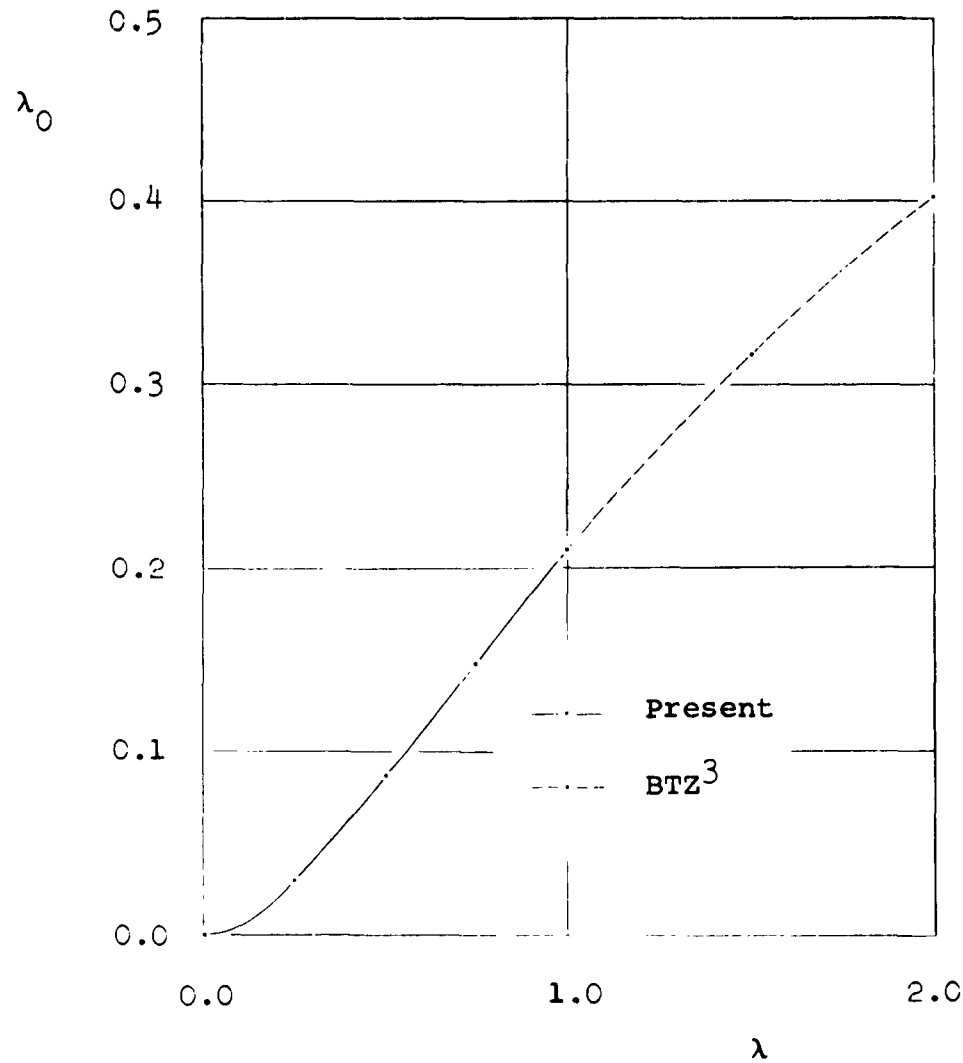

FIGURE 2.2

EXTREMUM EIGENVALUE λ_0 OF [P]

FOR ZEROTH HARMONIC

TABLE 2.5

EXTREMUM EIGENVALUE λ_0 OF [P]

λ	λ_0	
	PRESENT	BTZ
0.00	0.000	0.000
0.25	0.030	
0.50	0.086	0.086
0.75	0.148	
1.00	0.210	0.210
1.50		0.317
2.00		0.402

or

$$\bar{\Gamma} = (2/3\sqrt{3})\ (2 \sin \pi\hat{r} - \sin 2\pi\hat{r}) \qquad (2.31)$$

where $\hat{r} \equiv r/R_p$. It represents a disk loading, neglecting inflow, of 41.1 psf at U = 200 mph and STP. For the values of the parameters we take,

$$J = 1$$

$$N = 2$$

$$\bar{x}_p = 0$$

$$\epsilon_e = -1.0^\circ$$

$$\lambda = 2/3$$

$$\mu = 0.95 \qquad (2.32)$$

The corresponding geometrical shroud camber ϵ has been plotted in Fig. 2.3. The actual shape of the shroud can be obtained by numerical integration.

Only $c_{00}^{(0)}$ is different from zero. From Eqs. (2.14) and (2.20), the zeroth approximation to the Glauert coefficients of C_0 is

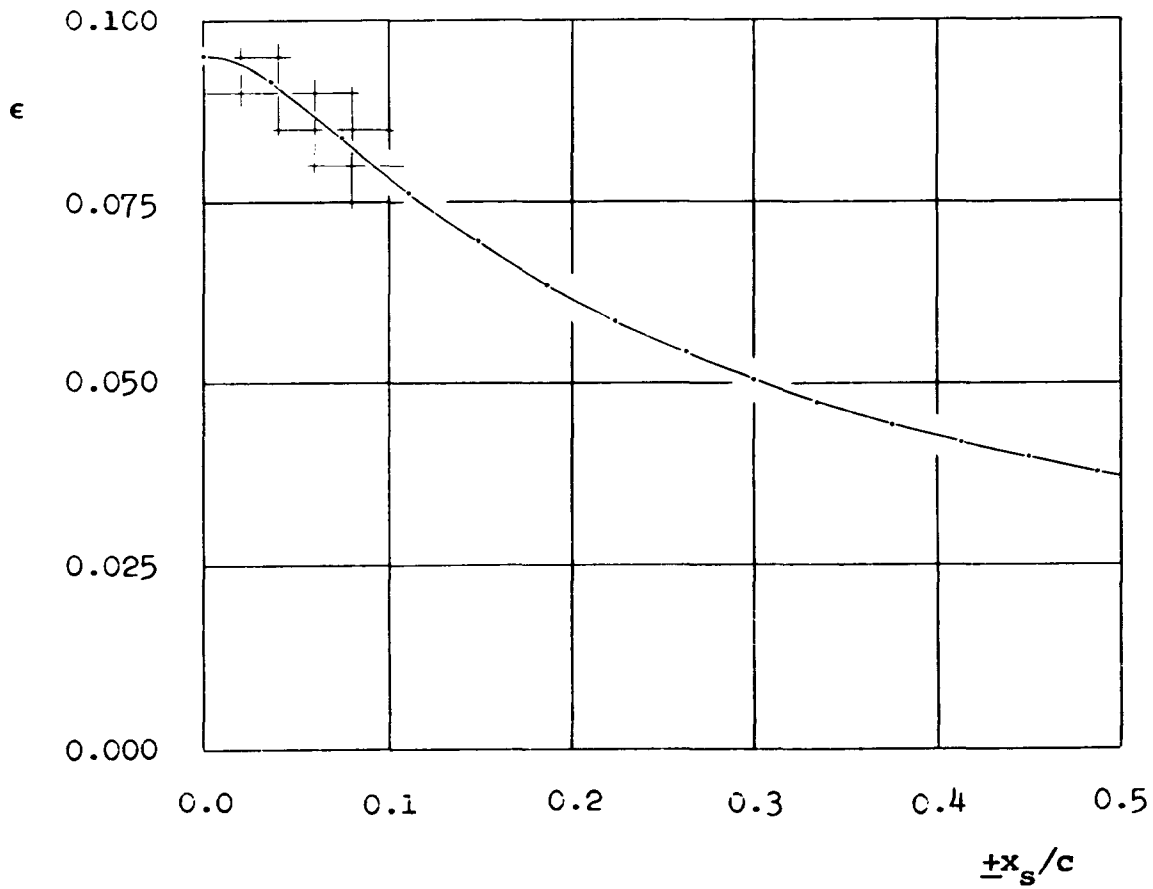

FIGURE 2.3

GEOMETRICAL SHROUD CAMBER FOR NUMERICAL EXAMPLE

$$\{c_0^{(0)}\} = \begin{Bmatrix} -0.0349 \\ 0.0000 \\ 0.0000 \\ \vdots \end{Bmatrix} \tag{2.33}$$

To find the values of $P_{k,\ell}$, we interpolate the data for $\lambda = 0.50$ and $\lambda = 0.75$ of Tables 2.2 and 2.3 and obtain

$$\begin{bmatrix} 0.104 & 0 & 0.052 & 0 & 0.000 & 0 & 0.000 \ldots \\ 0.208 & 0.126 & 0 & -0.023 & 0 & 0.000 & 0 \\ 0.045 & 0 & 0.030 & 0 & -0.008 & 0 & 0.000 \\ 0.000 & -0.008 & 0 & 0.011 & 0 & -0.004 & 0 \\ 0.000 & 0 & -0.004 & 0 & 0.006 & 0 & -0.002 \\ 0.000 & 0.000 & 0 & -0.002 & 0 & 0.004 & 0 \\ 0.000 & 0 & 0.000 & 0 & -0.001 & 0 & 0.002 \\ \vdots & & & & & & \end{bmatrix}$$

Now $\{c_0\}$ may be approximated by means of Eq. (2.23), the number of iterations determined consistent with $\{c_0^{(0)}\}$ and the accuracy afforded by $[P]$. This requires

$\lambda_0^{\,j} \leq 0.0005$ or $j = 4$ since $\lambda_0 = 0.128$, see Fig. 2.2. Accordingly, $([I] + [P] + \ldots [P]^4)$ is

$$\begin{bmatrix} 1.119 & 0 & 0.060 & 0 & 0.000 & 0 & 0.000 \ldots \\ 0.266 & 1.144 & 0.015 & -0.026 & 0 & 0.000 & 0 \\ 0.052 & 0 & 1.033 & 0 & -0.008 & 0 & 0.000 \\ -0.002 & -0.009 & 0 & 1.011 & 0 & -0.004 & 0 \\ 0.000 & 0 & -0.004 & 0 & 1.006 & 0 & -0.002 \\ 0.000 & 0.000 & 0 & -0.002 & 0 & 1.004 & 0 \\ 0.000 & 0 & 0.000 & 0 & -0.001 & 0 & 1.002 \\ \vdots & & & & & & \end{bmatrix}$$

and

$$\{c_0\} = \begin{Bmatrix} -0.0391 \\ -0.0093 \\ -0.0018 \\ 0.0001 \\ \vdots \end{Bmatrix} \qquad (2.34)$$

These results are substituted into the Glauert series and the difference in the average pressure coefficient across the shroud $\bar{c}_{p}]$, taken positive radially outward, is computed from the relation[1],

$$\bar{c}_{p}] = - 2\, c_{0} \tag{2.35}$$

It has been plotted in Fig. 2.4, together with the corresponding distribution for the effective airfoil in two-dimensional flow, i.e. $j = 0$. The influence of the shroud curvature is about 39% at the midchord.

In Table 2.6 we have also presented $\bar{c}_{p}]$ for each step in the iteration process to show the speed of convergence and to verify the accuracy of the solution.

2.6 Direct Inversion

J. Weissinger first achieved an exact solution to the ring airfoil problem by direct inversion[2]. His solution may be related to our iteration procedure in the following manner.

When a Neumann series converges, we know that the limit is expressible as an inverse matrix[8], or

$$([I] - [P])^{-1} = [I] + [P] + [P]^{2} + \ldots \tag{2.36}$$

as $j \to \infty$, then, Eq. (2.23) becomes from Eqs. (2.4) and (2.36)

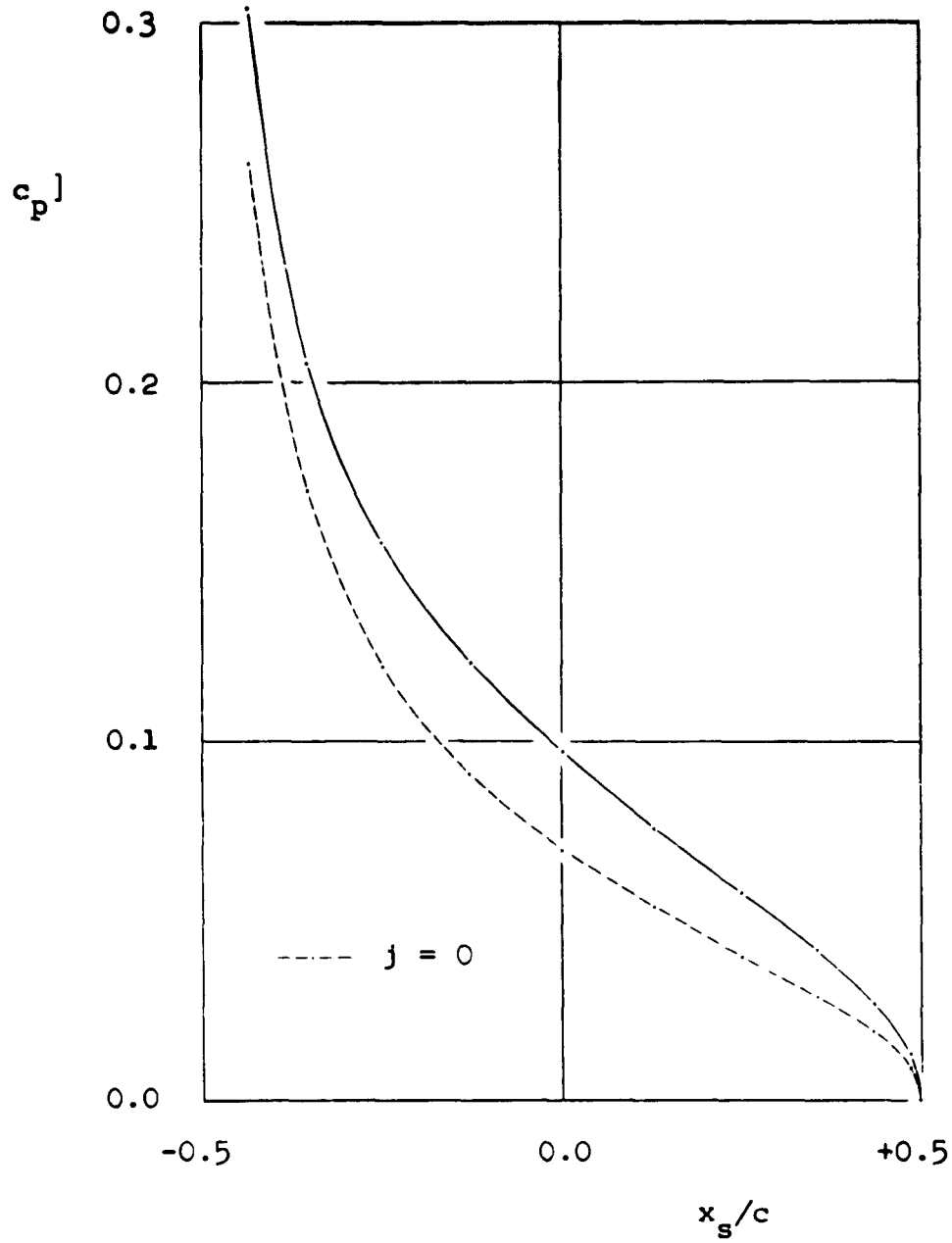

FIGURE 2.4

NET AVERAGE PRESSURE DISTRIBUTION ON THE SHROUD

$J = 1,\ N = 2,\ \bar{x}_p = 0,\ \epsilon_e = -1.0°,\ \lambda = 2/3,\ \mu = 0.95$

$\bar{\Gamma} = (2/3\sqrt{3})\ (2 \sin \pi\hat{r} - \sin 2\pi\hat{r})$

TABLE 2.6

$\bar{c}_p]$ AT EACH SUCCESSIVE STEP IN THE ITERATION PROCESS

	$\bar{c}_p]$				
x_s/c	j=0	j=1	j=2	j=3	j=4
-0.500	∞	∞	∞	∞	∞
-0.483	0.530	0.590	0.599	0.600	0.600
-0.433	0.261	0.297	0.303	0.304	0.304
-0.354	0.169	0.199	0.204	0.205	0.205
-0.250	0.121	0.149	0.154	0.155	0.155
-0.129	0.091	0.116	0.121	0.122	0.122
0	0.070	0.092	0.096	0.097	0.097
0.129	0.054	0.072	0.075	0.076	0.076
0.250	0.040	0.054	0.057	0.058	0.058
0.354	0.029	0.039	0.041	0.042	0.042
0.433	0.019	0.025	0.026	0.027	0.027
0.483	0.009	0.012	0.013	0.013	0.013
0.500	0	0	0	0	0

$$\{c_0\} = ([I] - [P])^{-1} \{c_0^{(0)}\} \tag{2.37}$$

This is the same as Weissinger's result gotten by substituting a Glauert series simultaneously into both sides of Eq. (2.2) and equating like cosine terms, cf. Eq. (2.19) without the superscripts (j) and $(j-1)$.

The form of Eq. (2.37) permits two conclusions: (i) The difference in average pressure across the shroud is identical to that of an equivalent airfoil with a modified camber in two-dimensional flow. To derive the modified camber, we determine the three-dimensional coefficients and replace them for the corresponding two-dimensional values in Eq. (2.13). (ii) Since we know the solution by direct inversion exists, the inverse matrix $([I] - [P])^{-1}$ must exist and $|[I] - [P]| \neq 0$. Consequently, comparison with Eq. (2.29) precludes the possibility that $\lambda_0 = 1$.

Either iteration or direct inversion may be used in any application, each becoming progressively cumbersome as λ increases. For numerical purposes, iteration affords a simple evaluation of the computational accuracy and minimizes the chances for arithmetical errors.

CHAPTER THREE

HIGHER HARMONIC SOLUTIONS

3.1 Methods of Approach

Neither the iteration process nor the equivalent direct inversion of Eq. (1.4) for the zeroth harmonic depends upon the nature of the regular part of the kernel. Therefore, if we can decouple Eqs. (1.10) for the higher harmonics into a form with a kernel which has a similar Cauchy singularity, we can utilize the same technique. Fortunately, we found such a way to decouple these equations earlier[1] and so have a solution in effect for the higher harmonics.

An alternate method of solution is possible by direct inversion of the coupled integral equations. That is, we follow the development of the integral of the product of the Glauert series and the kernel function itself, as well as its derivative, into a cosine series in ϕ and then, determine simultaneously the coefficients of like terms.

Generally speaking, either of these approaches is quite complicated. One simplification is achieved, though, if we take the limit of infinite advance ratio. In this case $B_1, B_2, B_3, \ldots \equiv 0$ and the integral equation for $A_1, A_2, A_3, \ldots$ is the same as for an equivalent asymmetric ring wing at zero angle of attack in uniform flow, the

effective asymmetry arising from the circumferential variation of radial velocity induced by the propeller. Accordingly, such a limit is of particular interest to assess the importance of the higher harmonics and to check the computational procedures of numerical programs.

3.2 Solution by Reduction to Zeroth Harmonic Form

We will only outline here the reduction of the coupled equations to the zeroth harmonic form.

We let the second integrals on the right hand side of Eqs. (1.10) be denoted by I_A and I_B respectively. Since the derivative of $K_m(\Delta\bar{x}_v)$ with respect to $\Delta\bar{x}_v$ is equal to the derivative with respect to $\bar{x}_s$ which can be brought out from under the integral sign of the first integrals, Eqs. (1.10) so represent a set of first order, linear differential equations in $\bar{x}_s$. To separate I_A, we take the derivative of the first equation and subtract σ times the second; or to separate I_B, we multiply the first by σ and add to the derivative of the second. Both results are of the form of a second order, linear differential equation for a simple harmonic oscillator subject to a forcing function. That is, we view I_A and I_B as "particle displacements" and the axial coordinate $\bar{x}_s$ as "time". The "motion" is undamped with a "natural frequency" σ. The "forcing functions" are,

$$P_A \equiv (A_{\Gamma m} + A_{\Gamma',m})' - \sigma\,(B_{\Gamma',m})$$

$$P_B \equiv (B_{\Gamma',m})' + \sigma\,(A_{\Gamma m} + A_{\Gamma',m}) \qquad (3.1)$$

From these differential equations, solutions for I_A and I_B may be found separately which provide decoupled equations for A_M and B_M.

For the inhomogeneous solutions, we determine the "indicial response" to a unit step function and use Duhamel's method of superposition. If the resulting equations are differentiated with respect to $\bar{x}_s$ and the differentiation is carried back inside the integrals I_A and I_B, the final equations assume the form,

$$\int_{-\lambda}^{\bar{x}_s} P_A(\bar{x})\cos\sigma\bar{x}\,d\bar{x} = \int_{-\lambda}^{\lambda} A_m(\bar{x}_v)\,K_m'(\Delta\bar{x}_v)\,d\bar{x}_v$$

$$\int_{-\lambda}^{\bar{x}_s} P_B(\bar{x})\cos\sigma\bar{x}\,d\bar{x} = \int_{-\lambda}^{\lambda} B_m(\bar{x}_v)\,K_m'(\Delta\bar{x}_v)\,d\bar{x}_v \qquad (3.2)$$

Eqs. (3.2) are now identical in structure to Eq. (1.4) and yield to solution as before, though in detail they are quite complex.

Comparing the terms on the left hand side by means of

Eqs. (1.5), (1.6), (1.11) and (3.1), we see that several additional terms as well as two integrations, i.e. on $\bar{\tau}$ and $\bar{x}$, are involved. These integrations are further aggravated by the "integral" presence of the advance ratio J and the blade number N. In the zero harmonic, they appear simply as factors of the propeller contribution to ϵ_e.

On the other hand, the relative complexity of the terms on the right hand side of Eqs. (1.4) and (3.2) is not so great. Only a few more terms and an integration on $\bar{\tau}$ are imposed. Previously no parameters appeared in the kernel. Now we have J, μ, m and N or explicitly, the combinations $J\mu$ and mN, which along with λ enter in the curvature coefficients. We also notice that the kernel K_m' is not antisymmetric about $\Delta\bar{x}_v = 0$ because of $g_{mN}'(\Delta\bar{x}_v,1)$ or $h_{mN}(\Delta\bar{x}_v,1)$, see Eq. (1.12). This extends the calculation of the corresponding Fourier coefficients $p_{k,\ell}$ for the expansion of the regular part of the kernel $\tilde{\tilde{K}}_m'$ to include all values of k and ℓ, no coefficients vanishing identically.

Besides the inhomogeneous solutions to the differential equations for I_A and I_B, there are also homogeneous solutions. The corresponding load distributions which they produce may be found in the same way as the A_m and B_m for the inhomogeneous solutions, but the physical interpretation of these distributions is not yet clear.

3.3 Direct, Simultaneous Inversion

Rather than decouple the governing equations by differ-entiation, we can express them in matrix form as for the zero harmonic and solve by direct, simultaneous inversion, i.e. we assume both A_m and B_m in the form of a Glauert series

$$A_m = a_{m0} \frac{1 + \cos \phi}{\sin \phi} + \sum_{\nu=1}^{\infty} a_{m\nu} \sin \nu\phi$$

$$B_m = b_{m0} \frac{1 + \cos \phi}{\sin \phi} + \sum_{\nu=1}^{\infty} b_{m\nu} \sin \nu\phi \qquad (3.3)$$

and substitute in Eqs. (1.10). With suitable Fourier expansions of K_m and K_m' the integrals over A_m and B_m may be written as pure cosine series in the Glauert angular variable ϕ_s for the position on the shroud. The propeller terms $A_{\Gamma m}$, $A_{\Gamma' m}$ and $B_{\Gamma' m}$ can be expressed in a similar fashion. Equating like coefficients, we may write the set of linear equations in the Glauert coefficients as a matrix equation and invert.

As noted earlier, K_m has a logarithmic singularity, see S_{mN} of Eq. (1.14) and Eq. (1.8). Consequently, if we define a regular part $\tilde{\tilde{K}}_m$,

$$\tilde{\tilde{K}}_m \equiv K_m + \frac{1}{4\pi} \ell n \frac{\Delta \bar{x}_\nu^2}{2} \qquad (3.4)$$

the terms in K_m' may be reduced right away from the zeroth harmonic, or from Eqs. (2.1), (2.12), (2.15), (2.16), (2.17) together with Eqs. (3.3) and $\tilde{\tilde{K}}_m'$ expressed in the double Fourier series of Eq. (2.6), cf. Eqs. (2.13) and (2.37),

$$\int_{-\lambda}^{\lambda} A_m \, K_m' \, d\bar{x}_v = - \{\phi_s\}^T \, [O_{K'}] \, \{a_m\}$$

$$\int_{-\lambda}^{\lambda} B_m \, K_m \, d\bar{x}_v = - \{\phi_s\}^T \, [O_{K'}] \, \{b_m\}$$

$$[O_{K'}] \equiv [I] - [P] \tag{3.5}$$

The matrix $\{\phi_s\}^T$ is defined by,

$$\{\phi_s\}^T \equiv \frac{1}{2} \left\{ \begin{array}{c} 1 \\ -\cos \phi_s \\ -\cos 2\phi_s \\ \vdots \end{array} \right\}^T \tag{3.6}$$

where "T" denotes a transpose or row matrix. [I] is the unit matrix and [P] is the matrix of Eq. (2.21) having the elements of Eqs. (2.7) and (2.10) with $\tilde{\tilde{K}}'_m$ in place of $\tilde{\tilde{K}}'_0$. The remaining matrices $\{a_m\}$ and $\{b_m\}$ are column matrices of the form of Eq. (2.20) with the Glauert coefficients of Eqs. (3.3) respectively as elements.

For the reduction of the terms in K_m of Eqs. (1.10), we proceed in a similar manner and separate the singular and regular parts. The logarithmic term arises in the calculation of the average shroud pressure coefficient. It has been evaluated by means of integration by parts, along with the Glauert integrals of Eqs. (2.12) and a related integral[9]. The regular part may be expanded and written exactly as before. Thus,

$$\int_{-\lambda}^{\lambda} A_m K_m \, d\bar{x}_v = - \{\phi_s\}^T [O_K] \{a_m\}$$

$$\int_{-\lambda}^{\lambda} B_m K_m \, d\bar{x}_v = - \{\phi_s\}^T [O_K] \{b_m\}$$

$$[O_K] \equiv [J] - [Q] \tag{3.7}$$

The matrix [J] comes from the singular part and is given by,

$$[J] \equiv \begin{bmatrix} \frac{\lambda}{2}\ell n\frac{\lambda^2}{8} & \frac{\lambda}{4}\ell n\frac{\lambda^2}{8} & 0 & 0 & 0 & 0 & 0 & \cdots \\ \lambda & 0 & \lambda & 0 & 0 & 0 & 0 & \\ 0 & -\frac{\lambda}{4} & 0 & \frac{\lambda}{2} & 0 & 0 & 0 & \\ 0 & 0 & -\frac{\lambda}{3} & 0 & \frac{\lambda}{3} & 0 & 0 & \\ 0 & 0 & 0 & -\frac{\lambda}{4} & 0 & \frac{\lambda}{4} & 0 & \\ 0 & 0 & 0 & 0 & -\frac{\lambda}{5} & 0 & \frac{\lambda}{5} & \\ \vdots & & & & & & & \end{bmatrix} \qquad (3.8)$$

The matrix $[Q]$ from the regular part is analogous to $[P]$ in Eq. (3.5) with the elements $P_{k,\ell}$ replaced by $Q_{k,\ell}$ in Eq. (2.21), the Fourier coefficients $p_{k,\ell}$ by $q_{k,\ell}$ in Eq. (2.10), and $\tilde{\tilde{K}}'_0$ by $\tilde{\tilde{K}}_m$ in Eq. (2.7).

To complete the matrix form of Eqs. (1.10), we set

$$A_{\Gamma m} + A_{\Gamma' m} = \{\phi_s\}^T \{a_{\Gamma,\Gamma'}\}$$

$$B_{\Gamma' m} = \{\phi_s\}^T \{b_{\Gamma'}\} \tag{3.9}$$

where $\{a_{\Gamma,\Gamma'}\}$ and $\{b_{\Gamma'}\}$ are column vectors. The elements are derived from Eqs. (2.14) using $(A_{\Gamma m} + A_{\Gamma' m})$ and $B_{\Gamma' m}$ respectively instead of ϵ_e.

From these results and Eqs. (3.5) and (3.7), Eqs. (1.10) give

$$\{a_{\Gamma,\Gamma'}\} = -[Q_{K'}]\{a_m\} - \sigma[Q_K]\{b_m\}$$

$$\{b_{\Gamma'}\} = -[Q_{K'}]\{b_m\} + \sigma[Q_K]\{a_m\} \tag{3.10}$$

By suitable manipulation, we may solve and obtain,

$$\{a_m\} = \frac{-[Q_K]^{-1}\{a_{\Gamma,\Gamma'}\} + \sigma[Q_{K'}]^{-1}\{b_{\Gamma'}\}}{[Q_K]^{-1}[Q_{K'}] + \sigma^2[Q_{K'}]^{-1}[Q_K]}$$

$$\{b_m\} = \frac{-[O_K]^{-1}\{b_{\Gamma'}\} - \sigma[O_{K'}]^{-1}\{a_{\Gamma,\Gamma'}\}}{[O_K]^{-1}[O_{K'}] + \sigma^2[O_{K'}]^{-1}[O_K]} \qquad (3.11)$$

if we assume that all the inverse matrices exist. The matrix $[O_K]^{-1}$ can be removed by multiplication with $[O_K]$; and the matrix $[O_{K'}]^{-1}$ can be expanded as for the zeroth harmonic, see Eq. (2.40).

Eqs. (3.11), then, constitute the solution by this method. The homogeneous solutions correspond to Eqs. (3.10) with the terms $\{a_{\Gamma,\Gamma'}\}$ and $\{b_{\Gamma'}\}$ suppressed, requiring the determinant of the common denominator of Eqs. (3.11) to vanish.

3.4 Comparison of Methods

Which of these methods is better for numerical calculations is difficult to judge. The first method imposes an additional differentiation and integration of the propeller contributions, but the second method imposes the determination of the Fourier coefficients for both $\tilde{\tilde{K}}_m$ and $\tilde{\tilde{K}}'_m$. On the other hand, the total number of operations appear less for the first method, but the second method involves fewer types of operations.

By either method, the complexity of the calculations demand every simplification and utmost care. In particular, the limiting case of infinite advance ratio should be carefully checked. For this case the equations naturally decouple

and the kernel is related by Eq. (1.16) to Weissinger's function "U_m" which has been computed for three harmonics. The corresponding Fourier coefficients have been computed by the Bureau Technique Zborowski[3] over a range of values and the propeller terms have been simplified by explicit evaluation of the inner integrations over the wake.

CONCLUSIONS

An iteration procedure has been developed for the general harmonic solutions to the equations for the ducted propeller with finite blade number in uniform motion at zero incidence. Solutions have also been obtained by direct inversion.

The results for the zeroth harmonic or the average shroud load show:

- Each iterate is expressed in identical form and is given explicitly in terms of the effective sectional camber and the chord to diameter ratio.
- The iteration procedure reduces to a matrix form which permits rapid numerical calculations.
- The number of iterations required for a prescribed computational accuracy may be estimated a priori.
- The solution by iteration converges in the limit to the direct inversion of the ring airfoil problem by J. Weissinger.
- The distribution of the average static pressure difference across the shroud is identical to the load on the equivalent airfoil in two-dimensional flow.

The results for the higher harmonics reveal:

- The equations may be decoupled into the same form as the equation for the zeroth harmonic and solved by iteration.
- An alternative method for solution by direct, simultaneous inversion appears to offer more promise for future studies.

The inherent complexity of these harmonics requires careful consideration of their significance to design before their calculation is attempted.

To assess the magnitude of these harmonics and to check out any computational program for them, the special case of infinite advance ratio is recommended for initial evaluation.

The iteration procedure may be applied to several other problems; for example, the two-dimensional airfoil in a bounded stream[10] and the translational characteristics of the GEM[11]. It affords not only important physical insight, but also marked simplicity.

REFERENCES

1. Ordway, D. E., Sluyter, M. M., and Sonnerup, B. O. U., Three-Dimensional Theory of Ducted Propellers, THERM, Incorporated, TAR-TR 602, August 1960.

2. Weissinger, J., Zür Aerodynamik der Ringflügels in inkompressibler Strömung, Zeitschrift für Flugwissenschaften, Heft 3/4, pp. 141-150, March/April 1956.

3. Ladurner, O., Theoretical Investigation and Examination by Measuring Tests in What a Degree the Economy of Flying Vehicles is Influenced by Pre-Cambered Skeletons of Airfoils Closed in Themselves, Bureau Technique Zborowski, DA-91-508-EUC393, August 1959.

4. Sonnerup, B. O. U., Expression as a Legendre Function of an Elliptic Integral Occurring in Wing Theory, THERM, Incorporated, TAR-TN 59-1, November 1959.

5. Sluyter, M. M., A Computational Program and Extended Tabulation of Legendre Functions of Second Kind and Half Order, THERM, Incorporated, TAR-TR 601, August 1960.

6. Bartholomew, G. E., Numerical Integration Over the Triangle, Mathematical Tables and Other Aids to Computation, pp. 295-298, October 1959.

7. Glauert, H., The Elements of Aerofoil and Airscrew Theory, 2nd Edition, Cambridge, pp. 87-93, 1948.

8. Courant, R., and Hilbert, D., Methods of Mathematical Physics, 1st English Edition, Volume 1, Interscience Publishers, Inc., 1953.

9. Hough, G. R., The Aerodynamic Loading on Streamlined Ducted Bodies, THERM, Incorporated; to be published.

10. Green, A. E., The Two-Dimensional Airfoil in a Bounded Stream, The Quarterly Journal of Mathematics (Oxford), 18, pp. 167-177, 1947.

11. Royce, W. W., and Rethorst, S., Translational Characteristics of Ground Effect Machines, IAS Paper No. 61-79, January 1961.